False Activation in Partially Sampled Dual-Task fMRI

Mary C. Kociuba[1], Daniel B. Rowe[1,2]

[1]Department of Mathematics, Statistics, and Computer Science, Marquette University, Milwaukee, WI, USA

[2]Department of Biophysics, Medical College of Wisconsin, Milwaukee, WI, USA

Abstract

To increase k-space acquisition speed and reduce variability inherent within the acquired signal, accelerated imaging techniques and signal processing operations are implemented before statistical analysis of functional MRI (fMRI) data. In this study, the spatial correlations of partially sampled dual-task k-space data are estimated in terms of temporal frequencies. Given a dual-task experimental design with different task periods, two distinct task-activated peaks are expected. Although, processing operations and parallel reconstruction methods generally induce correlations, through spreading voxel task-activated peaks temporally and spatially into neighboring frequencies and voxels. If the period of both tasks falls within a close range, correlation will be induced between voxels activated by different tasks, as a result of increased overlapping frequency content. A comparison of fully and partially sampled k-space will yield artificial spatial correlations and false activation, as a result of induced task-activated peaks in previously aliased regions. Without knowledge of the expected task-activated regions, it is difficult to resolve the task to the associated region after processing.

Key Words: pMRI, fMRI

1. Introduction

In fMRI, the measured blood oxygen level dependent (BOLD) signal used to detect neural activity is spatially Fourier encoded [1,2]. The reconstructed image is the inverse Fourier transform of the acquired complex-valued k-space data. With parallel reconstruction methods, data acquisition timing is optimized resulting in faster observation of brain function. To mitigate noise inherent from data acquisition procedures and unwanted physiological sources, processing operations are applied before the statistical analysis of the data. Although, it is well documented that parallel reconstruction techniques and signal processing operations modify a voxel's temporal spectrum and generally induces correlation [3-6]. Specifically, parallel image reconstruction methods associated with accelerated imaging, SENSitivity Encoding (SENSE) [7] and Generalized Autocalibrating Partially Parallel Acquisition (GRAPPA) [8], have also been shown to induce long range spatial correlation between previously aliased voxels [9,10]. In this study a Fourier frequency framework is described where the spatial correlations induced from parallel image reconstruction procedures are represented in terms of temporal frequencies. This representation of correlations is written as a summation of temporal frequencies, such that specific frequencies or portions of a voxel's temporal frequency spectrum that contribute substantially to spatial correlation are identified.

The linear relationship between the image domain and spatial frequency domain is the basis for this study, and critical to describing the statistical implications of signal processing and reconstruction in fMRI studies. The spatial correlations are described as a linear combination of second order voxel temporal frequencies using both the magnitude and phase components of the data [11]. The standard in fMRI analysis is to discard the phase portion of the data and implement a magnitude-only (MO) analysis to detect regions of activation [12,13]. In comparison, executing a complex-valued (CV) model in fMRI analysis has shown to detect increased regions of activation [14,15]. Including phase information in the data increases the statistical power of the model. While both MO and CV models describe activation in the image domain, analysis within the frequency domain is valuable. It has previously been shown how complex-valued temporal frequencies contribute to the correlations between voxels in the cerebral cortex for magnitude-only non-task data [16]. The complex-valued frequency description of correlation, compared to the MO or CV time-series correlation, allows the correlation to be divided into distinct partitions. This property of the Fourier temporal frequency framework derived in this manuscript is valuable for examining the residual signal leakage from accelerated data acquisition and reconstruction methods. For example, with subsampled data with an in-plane acceleration factor of 3, three voxels will initially have the same voxel location before separation. The nature of the acquisition of this data and correlation induced during the separation process with SENSE or GRAPPA, results in aliasing artifacts of signal leakage among the three aliased voxels.

In this manuscript, the utility of this temporal Fourier frequency representation of spatial correlation is established with a simulation of dual-task fMRI data and SENSE reconstruction. Given a dual-task experimental design with different task periods, two distinct task-activated peaks are expected. Signal processing will alter the activated voxel's temporal frequency spectrums, by spreading voxel task activated peaks temporally and spatially into local frequencies and voxels. Previously aliased voxels from subsampling during accelerated data acquisition, will also have increased overlapping frequency content as a result of the parallel MRI reconstruction techniques. If the frequency of the two tasks fall within a close range, false activation among voxels activated by different tasks, may be detected as a result of increased overlapping frequency content. The application of the theory to complex-valued data validates the increased statistical power of using complex-valued models. Identifying frequencies contributing to induced correlations is critical for developing methods to remove noise, such that the signal of interest is preserved, and accurate conclusions are drawn from the subsampled data.

2. Background & Theory

2.1 The SENSE Model

In fMRI, the common parallel image reconstruction methods for in-plane acceleration include SENSE and GRAPPA. SENSE is an image space model and GRAPPA is a k-space model. The framework described in this work will be demonstrated with SENSE, which reduces scan time with use of phased receiver coil arrays and omitting measurements of the k-space readout, as illustrated in Figure 1. The receiver coils are necessary to remove the "fold over" artifacts, a result of failure to meet the Shannon-Nyquist sampling criteria, as seen in Figure 2a for an acceleration of 1, 2 and 4, and thus spatially compensate for the skipped lines in k-space. As seen in Figure 1a, a fully sampled k-space array corresponds to an acceleration factor of $A=1$, increasing the

acceleration factor corresponds to a distance between acquired lines of $A\Delta k_y$ as seen in Figure 1b and 1c.
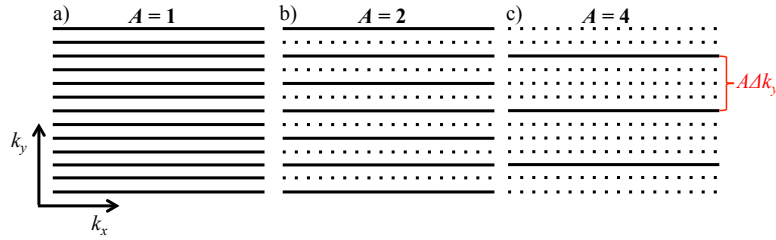
Figure 1: Acquisition of **a)** full k-space with $A = 1$, **b)** k-space subsampled with $A = 2$ in the PE direction, and **b)** k-space subsampled with $A = 4$ in the PE direction. Sampled lines are marked with a straight line, and dotted lines are the skipped lines of k-space.

   The receiver coil sensitivity profiles are estimated from fully sampled calibration images, and required to compensate for the missing phase encoding lines in the subsampled arrays. The complex-valued coil sensitivity maps are normalized in each voxel through averaging the coil sensitivity maps then dividing by a time-series calibration average sensitivity from each voxel. Optimal coil geometry and distinct coil sensitivity profiles of aliased voxels, leads to improved images during the voxel separation. Figure 2b is an illustration of the magnitude of four coils, each coil located on the four sides of the slice. Using multiple phased coils instead of a single coil to cover the same volume increases the signal-to-noise ratio (SNR) by increasing the number of averages for each image. However, as the number of coils is increased the sensitivity at each coil is reduced, thus there is an optimal SNR and noise trade-off regarding the number of coils used in MR imaging studies.
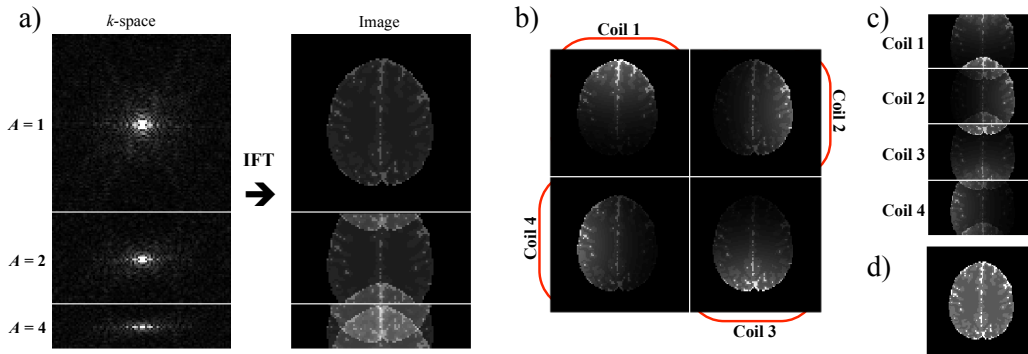
Figure 2: Acquisition and reconstruction to image space of **a)** k-space readout with $A = 1$, 2, and 3, **b)** illustration of the magnitude coil spatial locations in a four coil acquisition scheme, **c)** aliased slice images reconstructed with $A=2$, at each receiver coil located as in (b), and **d)** the slice image reconstructed from (c) and coil sensitivity profiles.

   An aliased slice with a subsampled k-space readout of $A=2$ measured at each receiver coil, configured as in Figure 2b, at a given time repetition (TR) is illustrated with Figure 2c. For N_C receiver coils, the complex-valued coil sensitivities at the jth coil measuring the zth voxel location is represented as $S_{jz}=S_{jRz}+iS_{jIz}$, where i is the imaginary unit. Voxel z in the aliased coil images is described with a complex-valued vector $a_{jz}=a_{jRz}+ia_{jIz}$ of N_C voxel measurements from the sub-sampled spatial frequencies, that are derived by $a_{jz} = S_{jz}v_{jz} + \varepsilon_{jz}$. Here $S_{jC} = S_{jR}+iS_{jI}$ is an $N_C{\times}A$ matrix with the fully sampled complex-

valued coil sensitivities, the magnitude is illustrated in Figure 2b, for the A aliased voxels in the N_C coils, $v_{jC}=v_{jR}+iv_{jI}$ is a vector of the A complex-valued un-aliased voxel values, and $\varepsilon_{jC}=\varepsilon_{jR}+i\varepsilon_{jI}$ is a vector of the N_C complex-valued additive measurement noise in each aliased voxel.

The aliased slice acquired at each coil is unstacked and reconstructed, through a least squares estimation with the fully sampled coil sensitivity maps. Thus, the images are measured as illustrated with Figure 2c for a single TR, then using the spatial information of the complex-valued coil sensitivity profiles the images are reconstructed as in Figure 2d. In the SENSE reconstruction model, the SNR is not uniform throughout the reconstructed image, and SENSE is often implemented with an acceleration of only 2 or 3. In this manuscript, an fMRI simulation with an acceleration factor of 3 is used.

2.2 A Complex-Valued Fourier Description of Covariance

In this section, the complex-valued Fourier frequency representation is derived to describe how signal processing and image reconstruction methods alter the structure of the spatial covariance matrix. Compared to magnitude-only correlations, applying this framework with complex-valued data more accurately identifies regions of spatial correlation, and reduces the noise in correlation maps.

When a $p_{row} \times p_{col}$ matrix of complex-valued k-space data S_t is a measured at time t, the usual process to reconstruct it into an image without any processing is to compute the discrete inverse Fourier transform (IFT). The IFT image reconstruction process for S_t is to pre-multiply it by a $p_{row} \times p_{row}$ complex-valued inverse Fourier transform matrix Ω_y and post-multiply it bythe transpose of a $p_{col} \times p_{col}$ complex-valued IFT matrix Ω_x. The jkth element of the $p_{col} \times p_{col}$ Fourier matrix Ω_x is $(\Omega_x)_{jk} = w^{(-\frac{pcol}{2}+j)(-\frac{pcol}{2}+k)}$ where j and k have indexing values from 0 to p_{col}-1 with $w = \frac{1}{N}e^{i2\pi/N}$ for the IFT and $w = e^{-i2\pi/N}$ for the forward Fourier transform (FT). To build up the needed real-valued matrix framework, consider the representation of the inverse Fourier reconstruction operator,

$$\Omega = \begin{bmatrix} \Omega_R & -\Omega_I \\ \Omega_I & \Omega_R \end{bmatrix} \tag{1}$$

where Ω_R and Ω_I are constructed with the use of the Kronecker product, $\Omega_R = [(\Omega_{yR} \otimes \Omega_{xR}) - (\Omega_{yI} \otimes \Omega_{xI})]$ and $\Omega_I = [(\Omega_{yR} \otimes \Omega_{xI}) + (\Omega_{yI} \otimes \Omega_{xR})]$ [17]. Upon representing the matrix of complex-valued spatial frequencies S_t as vector s_t by stacking the rows of the reals upon the rows of the imaginaries, a reconstructed image vector v_t can be formed that contains the rows of the reals stacked upon the rows of the imaginaries. A complex-valued image V can be made by unstacking every p_{col} elements into rows for reals then rows for imaginaries.

The observed k-space data acquired over n time repetitions (TRs) can be similarly represented. In this framework, the complex-valued spatial frequencies are represented in a real-valued $2pn\times1$ vector, s, with the rows of real voxel values of each image stacked over the corresponding rows of the imaginary voxel values for p voxels. An analogous explanation describes the organization of the real-valued reconstructed image $2pn\times1$ vector, v. The signal vector is reconstructed to the image vector, with the inverse Fourier reconstruction operator, Ω, in Eq. (1) with p_{row} and p_{col}, and the Kronecker product,

$$v = (I_n \otimes \Omega)s. \tag{2}$$

A $2pn \times 2pn$ permutation matrix, P, reorders the elements of vector v such that, $y = Pv$, and the real-valued time series $2pn \times 1$ vector y is now ordered by voxel rather than ordered by image. The voxel ordered time-series vector y is Fourier transformed into the temporal frequency domain, with the $2n \times 2n$ temporal forward Fourier transform matrix, $\overline{\Omega}_T$. The bar denotes the FT rather than the IFT, and the subscript signifies the temporal dimension such that the Fourier matrix operator is constructed with n rows and 1 column. The real-valued $2pn \times 1$ vector f consists of the temporal frequencies of each voxel stacked upon the corresponding imaginary temporal frequencies is represented,

$$f = \left(I_p \otimes \overline{\Omega}_T\right)Pv. \tag{3}$$

Thus, the real-valued vector and matrix representation in Eq. (3) describes the reconstruction process as a linear combination of matrix and vector multiplications.

Define a $2pn \times 1$ real-valued voxel time series with real parts stacked over imaginary parts for voxel j as y_j, which is reconstructed similar to Eq. (2) with a temporal IFT matrix, Ω_T, from its spatial frequencies, f_j, $y_j = \Omega_T f_j$. Comparable notation to describe an additional voxel k, and the spatial covariance between the two voxels is represented as

$$\text{cov}(y_j, y_k) = \frac{1}{2n}\left(y_j - \mu_{yj}\right)'\left(y_k - \mu_{yk}\right) = \frac{1}{2n}\tilde{y}_j' \tilde{y}_k,$$

where the demeaned time-series are represented as $\tilde{y}_j$ and $\tilde{y}_k$. If $\tilde{y}_j = \Omega_T \tilde{f}_j$, the time series correlation between two voxels,

$$\text{cov}(y_j, y_k) = \frac{1}{2n}\left(\Omega_T \tilde{f}_j\right)'\left(\Omega_T \tilde{f}_k\right) = \frac{1}{4}\tilde{f}_j' \tilde{f}_k = \frac{1}{4}(\tilde{f}_{jR}' \tilde{f}_{kR} + \tilde{f}_{jI}' \tilde{f}_{kI}), \tag{4}$$

which is described in terms of the real and imaginary components for each voxel temporal frequency spectrum. This notation is extended to describe spatial correlation between the two voxels,

$$\text{corr}(y_j, y_k) = \frac{\text{cov}(y_j, y_k)}{\sqrt{\text{var}(y_j)\text{var}(y_k)}} = \frac{\tilde{f}_{jR}' \tilde{f}_{kR} + \tilde{f}_{jI}' \tilde{f}_{kI}}{\sqrt{(\tilde{f}_{jR}' \tilde{f}_{jR} + \tilde{f}_{jI}' \tilde{f}_{jI})(\tilde{f}_{kR}' \tilde{f}_{kR} + \tilde{f}_{kI}' \tilde{f}_{kI})}}. \tag{5}$$

The spatial covariance in Eq. (4) can be expanded to a $p \times p$ spatial covariance matrix, Σ, such that the entry (j,k) in Σ represents the spatial covariance between two demeaned real-valued represented voxel time series of voxel j and voxel k,

$$\Sigma = \frac{1}{4}\begin{bmatrix} \tilde{f}_{1R}' \tilde{f}_{1R} + \tilde{f}_{1I}' \tilde{f}_{1I} & \cdots & \tilde{f}_{1R}' \tilde{f}_{pR} + \tilde{f}_{1I}' \tilde{f}_{pI} \\ \vdots & \ddots & \vdots \\ \tilde{f}_{pR}' \tilde{f}_{1R} + \tilde{f}_{pI}' \tilde{f}_{1I} & \cdots & \tilde{f}_{pR}' \tilde{f}_{pR} + \tilde{f}_{pI}' \tilde{f}_{pI} \end{bmatrix}, \tag{6}$$

Additionally, Eq. (5) is also expanded to matrix form to represent p voxels, by defining D as the diagonal matrix consisting of the diagonal elements of Σ as in Eq. (6). A symmetric $p \times p$ spatial correlation matrix constructed from the spatial covariance is formed with the multiplication

$$R = D^{-1/2} \Sigma D^{-1/2}. \tag{7}$$

By aggregating the second order temporal frequencies into biologically meaningful or experimentally relevant bands, the influence processing steps and reconstruction algorithms have on each voxel's temporal frequency spectrum can be quantitatively measured. In an fMRI study, the frequency corresponding to the activation is considered when dividing the spectrum into bands. Note in this study, the temporal spectrum is not divided evenly into bands, since each band has a varying degree of relevance to the study. To understand the contribution each temporal frequency band yields to spatial correlation, the correlation is expressed as,

$$r_b = \frac{(\tilde{f}'_{jR}\tilde{f}_{kR} + \tilde{f}'_{jI}\tilde{f}_{kI})_b}{\sqrt{\sum_{\ell=1}^{p_b}(\tilde{f}'_{jR}\tilde{f}_{jR} + \tilde{f}'_{jI}\tilde{f}_{jI})_\ell \sum_{\ell=1}^{p_b}(\tilde{f}'_{kR}\tilde{f}_{kR} + \tilde{f}'_{kI}\tilde{f}_{kI})_\ell}},$$

where the numerator consists of the covariance between two voxel's demeaned temporal frequency spectrums for a frequency band b, the denominator is the variance of each voxel's temporal spectrum, and p_b is the total number of bands. The spatial covariance matrix can be written as a summation of covariance of each band

$$\Sigma = \Sigma_1 + \cdots + \Sigma_{p_b},$$

and the Eq. (7) spatial correlation matrix can be written as a summation of correlation of bands

$$R = D^{-1/2}(\Sigma_1 + \cdots + \Sigma_{p_b})D^{-1/2}.$$

In addition to analyzing the spatial correlation as bands, observing the spectral decomposition for each voxel of interest provides visual insight to the potential temporal frequency contribution for each voxel towards the spatial correlation. For the ℓth band in the temporal frequency spectrum for any voxel, the potential spatial correlation contribution of that frequency is described as

$$r_\ell = \frac{\tilde{f}^2_{jR_\ell} + \tilde{f}^2_{jI_\ell}}{\tilde{f}'_{jR}\tilde{f}_{jR} + \tilde{f}'_{jI}\tilde{f}_{jI}} . \tag{8}$$

Note, r_ℓ describes the correlation contribution at each temporal frequency such that $\sum_{\ell=1}^{n} r_\ell = 1$.

3. Methods

In MATLAB (Mathworks, Natick, MA), a T_2^* weighted 96×96 digital phantom [18] with a 240 mm field of view (FOV) is generated with 720 TRs, with an in-plane acceleration $A = 3$. The data is generated with an SNR equal to 20, and the contrast-to-noise ratio (CNR) equal to ½. Four coils are located on the sides and the images are SENSE reconstructed. Complex-valued activation is simulated with a sinusoid added to the magnitude time-series, and a phase shift is added to the phase time-series for three 4×4 voxel blocks in located in the aliased positions in the phantom, as describe in Figure 3. There are two tasks between the three voxel locations, where task 1 corresponds to a

task of fifteen 24-second periods, and task 2 corresponds to sixteen 22-second periods. The data is processed with spatial smoothing using a Gaussian kernel with a full-width-half-max (FWHM) of 2 voxels. The temporal spectrums are high-pass band filtered (<0.009 Hz), and low-pass band filtered (>0.08 Hz). For the analysis, three voxels, one from each 4×4 voxel block, are analyzed. The spatial correlations in terms of the voxel temporal spectrums are analyzed with and without the in-plane subsampling, and complex-valued activation [15] is computed for each task design.

Figure 3: The two tasks are assigned and the three voxel blocks are chosen based on the overlapping aliased voxel location as illustrated in the figure.
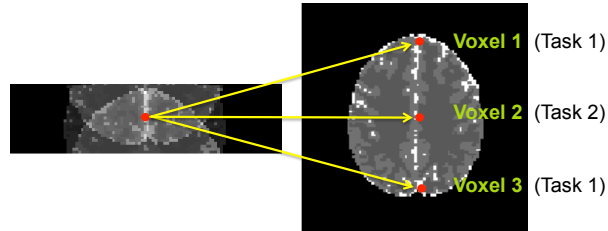
4. Results

The peaks in Figure 4a are associated with task period assigned to each voxel location. In this dual-task fMRI simulation, since the two tasks are performed at different periods, two distinct task-activated peaks are expected. Since both task-activated peaks fall within a close range, correlation will be induced between voxels activated by different tasks, as a result of increased overlapping frequency content from the reconstruction process. As expected from examining the temporal frequency decomposition, there is signal leakage from the SENSE un-aliasing, between the dual-task locations, apparent in the z-statistic activation maps, as shown in Figure 4b.
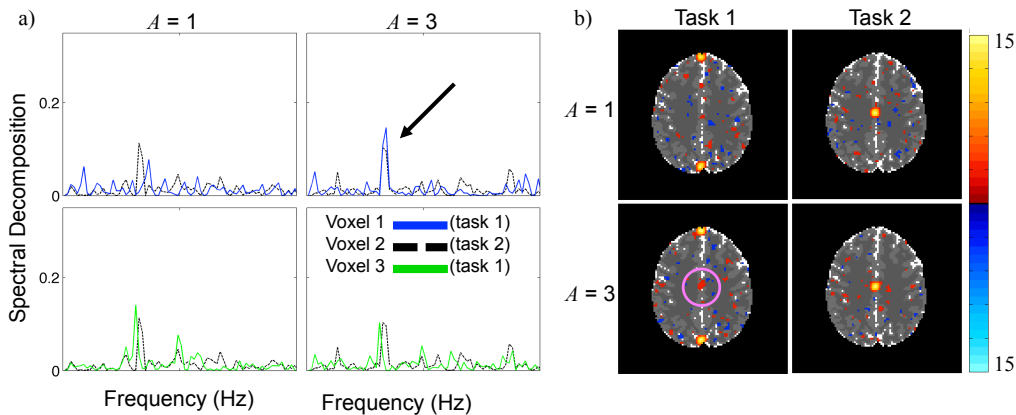
Figure 4: a) The correlation contribution using Eq. 8 of the 3 voxel temporal frequency spectrums, with and without an in-plane acceleration of $A = 3$, **b)** complex-valued task activation for the task 1 and task 2 block designs, with and without an in-plane acceleration of $A = 3$.

Figure 4a is a visualization of the correlation contribution at each frequency, so that the sum of the values for each voxel's spectrum equals 1, as developed in Eq. (8). Thus the more overlapping content between the two voxel's temporal spectrums, the stronger spatial correlation between the two voxels. With in-plane acceleration of $A=3$, as shown in Figure 4a, voxel 2, which is associated with task 2, shares an increased overlapping frequency content at the task-frequency with voxel 1 and voxel 3, which are associated

with task 1. Although, the spatial correlations look similar in Figure 5 between the two accelerations, there is a subtle increase in the correlation between the two voxels with the same task. This increase is expected, since SENSE reconstructed images have an increased SNR in neural regions previously aliased with other neural regions, compared to images acquired with no in-plane acceleration.
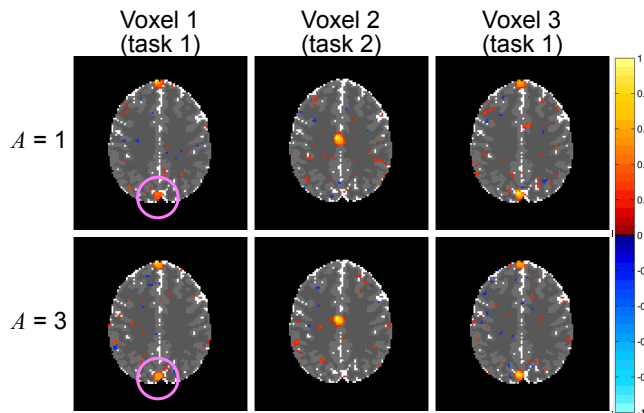
Figure 5: The spatial correlation maps with and without an in-plane acceleration of $A = 3$, for each voxel of interest.

5. Discussion and Conclusions

Temporal resolution is important to distinguish neural events through time, and spatial resolution is important for precisely identifying brain regions of interest. Although, achieving satisfactory spatial and temporal resolution is difficult. If more lines of k-space are measured for each slice acquisition, the time for successive acquisition of slices is extended, and spatial resolution is increased with reduced temporal resolution. If fewer lines of k-space are measured for each slice acquisition, the time for successive acquisition of slices is reduced, and spatial resolution is reduced with increased temporal resolution. Thus faster observation of brain function means a trade off between spatial and temporal resolution. Although, parallel MRI acquisition methods serve to improve temporal resolution, while mitigating aliasing artifacts between previously aliased voxels. Yet, reconstruction operations induce correlation between voxels activated by different tasks, as a result of increased overlapping frequency content. Strategic experimental design in parallel MRI (pMRI) models may be important to maintain minimal signal leakage in reconstructed images, such that conclusions from the statistical analysis are not impacted. Modeling functional MRI analysis around the frequency task peak, or considering the effects of processing or reconstruction on critical partitions of a voxel's temporal frequency spectrum, will strengthen the statistical power of the model. More specifically, this research may be applicable to functional connectivity MRI, since the biological correlation pattern in the default mode network (DMN) is similar to a SENSE aliasing pattern. Thus, it is important to distinguish between the processing and reconstructed induced correlation and the true underlying correlation from the biological signal of interest.

Acknowledgements

References

1. Ogawa, S., Lee, T.M., Kay, A.R., Tank, D.W. Brain Magnetic Resonance Imaging with Contrast Dependent on Blood Oxygenation. Proc. Natl. Acad. Sci. USA 1990; 87: 9868-9872.

2. Bandettini, P.A., Wong, E.C., Hinks, R.S., Tikofsky, R.S., Hyde J.S., Time Course EPI of human brain function during task activation. Magn. Reson. Med. 1992; 25:390-397.

3. Friston, K.J., Josephs O., Zarahan E., Holmes, A.P., Rouquette, S., Poline, J.B., To Smooth or Not to Smooth? Bias and Efficiency in fMRI Time-Series Analysis. NeuroImage 2000; 12, 196-208.

4. Nencka, A.S., Hahn, A.D., Rowe, D.B. A Mathematical Model for Understanding Statistical Effects of k-space (AMMUST-k) Preprocessing on Observed Voxel Measurements in fcMRI and fMRI. J. Neurosci. Meth. 2009;181: 268–282.

5. Karaman MM, Nencka AS, Bruce IP, Rowe DB. Quantification of the Statistical Effects of Spatiotemporal Processing of Nontask fMRI Data. Brain Connectivity 2014;4:649–661.

6. Davey C.E., Grayden, D.B., Egan, G.F., Johnston, L.A., Filtering Induces Correlation in fMRI Resting State Data. NeuroImage 2013; 64, 728-740.

7. Pruessmann KP, Weiger M, Scheidegger MB, Boesiger P. SENSE: Sensitivity Encoding for fast MRI. Magn Reson Med 1999;42:952–962.

8. Griswold MA, Jakob PM, Heidemann RM, Nittka M, Jellus V, Wang J, Kiefer B, Haase A. Generalized Autocalibrating Partially Parallel Acquisitions (GRAPPA). Magn Reson Med 2002;47:1202–1210.

9. Bruce, I.P., Karaman, M.M, Rowe, D.B. A Statistical Examination of the SENSE Reconstruction via an Isomorphism Representation. Magn. Reson. Imag. 2011;29, 1267-1287.

10. Bruce, I.P., Rowe, D.B. Quantifying the Statistical Impact of GRAPPA in fcMRI Data with a Real-Valued Isomorphism. IEEE Transactions on Medical Imaging 2014; 33, 495-503.

11. Cordes, D., Haughton, V.M., Arfanakis, K., Wendt, G.J., Turski, P.A., Moritz, C.H., Quigley, M.A., Meyerand, M.E., Mapping Functionally Related Regions of Brain with Functional Connectivity MR Imaging. J. of Am. NeuroRadiology. 2000; 21: 1636-1644.

12. Bandettini, P.A., Jesmanowicz, A., Wong, E.C., Hyde, J.S., Processing strategies for time course data sets in functional MRI of the human brain. Magn. Reson. Med. 1993; 30:161–173.

13. Cox, R.W., Jesmanowicz, A., Hyde, J.S., Real-time functional magnetic resonance imaging. Magn. Reson. Med. 1995; 33; 230–236.

14. Rowe, D.B., Logan, B.R. A complex way to compute fMRI activation. NeuroImage 2004; 23:1078-92.

15. Rowe, D.B. Modeling both the magnitude and phase of complex-valued fMRI data. Neuroimage 2005; 25:1310-24.

16. Cordes, D., Haughton, V.M., Arfanakis, K., Carew, J.D., Turski, P.A., Quigley, M.A., Meyerand, M.E. Frequencies Contributing to Functional Connectivity in the Cerebral Cortex in "Resting-state" Data. J. of Am. NeuroRadiology. 2001; 22: 1326-1333.

17. Rowe D.B., Nencka A.S., Hoffmann R.G. Signal and Noise of Fourier Reconstructed fMRI Data. J. Neurosci. Meth. 2007; 159:361–369.

18. Karaman, M.M., Bruce I.P., Rowe D.B. Incorporating relaxivities to more accurately reconstruct MR images. Magn Reson Imaging 2015;33:85–96.